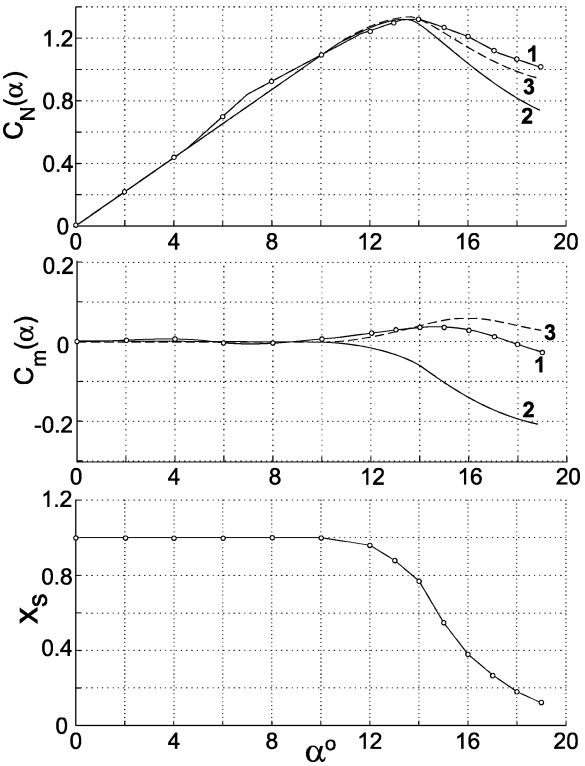

Fig. 6 Comparison of results for separated flow for NACA 0012 airfoil for $M = 0.15$ and $Re = 1 \times 10^6$ using XFOIL (1), the nonlinear theory (2), and the linear theory (3). In (2) and (3) the separation point location $x_s(\alpha)$ was prescribed from XFOIL output (lower part of the figure).

nonlinear behavior in $C_N(\alpha)$ and $C_m(\alpha)$. The linear and nonlinear analytic methods are in reasonable qualitative agreement with the XFOIL prediction of this nonlinear variation. Interestingly, the linear results happen to be in closer agreement with XFOIL than the nonlinear. Evidently, errors due to absence of airfoil thickness and the projection of boundary conditions onto the longitudinal axis to some extent cancel one another.

Conclusions

A solution, linear in angle of attack, is given for flow about a thin symmetric airfoil, that is, an inclined flat plate, with a semi-infinite separated region. This solution allows one to ascertain explicitly the effect of the development of upper-surface separation on the airfoil lift and pitching moment coefficients. The main drawback is the enforcement of the uniform-pressure boundary condition on the corresponding segments of the real axis, rather than on the actual boundary of the separated region. Physically, this assumes that the separated region is thin. Errors resulting from such an approximation were estimated by a comparison with the Chaplygin–Lavrientiev classical nonlinear solution. The linear solution was also compared with XFOIL results for a NACA 0012 airfoil. XFOIL's prediction of the location of the upper surface separation point was input into the analytic solutions, to obtain the static dependency of lift and pitching moment coefficients on angle of attack. Results from the linear and nonlinear analytic solution and the XFOIL computation were in satisfactory agreement.

Acknowledgments

Analytical investigations of airfoil flow separation with linear and nonlinear theories were supported by the Russian Federation Basic Research foundation RFBR Project 03–01–00918.

References

[1]Goman, M. G., and Khrabrov, A. N., "State-Space Representation of Aerodynamic Characteristics of an Aircraft at High Angles of Attack," *Journal of Aircraft*, 1994, Vol. 31, No. 5, pp. 1109–1115.

[2]Sedov, L. I., *Two Dimensional Problems in Hydrodynamics and Aerodynamics*, Wiley, New York, 1965, Chap. 2.

[3]Thwaites, B. (ed.), *Incompressible Aerodynamics*, Dover Publications, Mineola, NY, 1987.

[4]Woods, L. C., *The Theory of Subsonic Plane Flow*, Cambridge Univ. Press, Cambridge, England, U.K., 1961.

[5]Muskhelishvili, N. I., *Singular Integral Equations*, Noordhoff, Groningen, The Netherlands, 1953.

[6]Chaplygin, S. A., and Lavrentiev, A. L., "On the Lift and Drag of a Flat Wing of Infinite Span (Assuming Discontinuous Flow on its Upper Surface)," *Transactions of Central Aerohydrodynamics Institute*, No. 123, 1933.

[7]Drela, M., and Giles, M. B., "Viscous–Inviscid Analysis of Transonic and Low Reynolds Number Airfoils," *AIAA Journal*, Vol. 25, No. 10, 1987 pp. 1347–1355.

[8]Drela, M., "XFOIL: An Analysis and Design System for Low Reynolds Number Airfoils," Conf. on Low Reynolds Number Airfoil Aerodynamics, June 1989.

[9]Rayleigh, "On the Resistance of Fluids," Philosophical Magazine, Vol. 2, Ser. 5, 1876.

Limit-Cycle Oscillations of Swept-Back Trapezoidal Wings at Low Subsonic Flow

Saeed Shokrollahi* and Firooz Bakhtiari-Nejad†
Amirkabir University of Technology, 15875 Tehran, Iran

Introduction

THE effect of sweep angle and taper ratio of swept back trapezoidal wings based on geometrically nonlinear von Kármán plate theory is studied in this Note. A three-dimensional time-domain vortex lattice aerodynamic model is used to investigate the flutter characteristics and limit-cycle oscillations of a low aspect ratio swept back trapezoidal wing at low subsonic flow.

Flutter characteristics and nonlinear response of cantilevered, low-aspect ratio, rectangular and delta wing models in low subsonic flows have been studied recently. Hopkins and Dowell[1] and Weiliang and Dowell[2] studied the limit-cycle oscillations of rectangular cantilever plates in high supersonic flow. Their results provided good physical understanding about the flutter and limit-cycle oscillation characteristics for such plates in a high Mach number supersonic flow. Tang and Dowell[3] and Tang et al.[4] investigated limit-cycle oscillations of cantilever rectangular and delta plates at low subsonic flow. Their analysis included the vortex lattice theory in a reduced-order aerodynamic model. They investigated the effect of a steady angle of attack on both the flutter instability boundary and the limit-cycle oscillations. Bakhtiari-Nejad and Shokrollahi[5] conducted an aeroelastic eigenanalysis of a cantilever plate in low subsonic flow to predict flutter onset. The effect of local forcing functions on the response of a cantilever plate at low subsonic flow was also studied by Bakhtiari-Nejad et al.[6] In that paper, the piezoelectric actuators were used to model the local forcing functions and the effect of their positions on flutter suppression.

Theoretical Development

A plan view schematic diagram of a wing-plate geometry with a three-dimensional vortex lattice model of unsteady flow is shown in

Received 4 May 2003; revision received 1 March 2004; accepted for publication 19 March 2004.

*Ph.D. Student, Department of Mechanical Engineering.
†Associated Professor, Department of Mechanical Engineering.

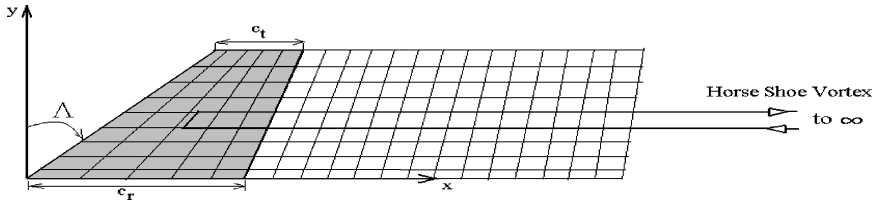

Fig. 1 Aeroelastic model of a swept back trapezoidal Cantilever plate.

Fig. 1. The fully coupled aeroelastic model is developed hereafter as a series of state-space equations. First, a nonlinear structural model of the wing is developed based on the von Kármán thin plate theory and Rayliegh–Ritz method. Next, the unsteady aerodynamic equations governing the three-dimensional flow about the model swept back trapezoidal wing are derived. Finally, the aeroelastic state-space equations are developed by coupling the structural dynamics equations with aerodynamic flow field.

Nonlinear Structural Model of Trapezoidal Wing

The swept back trapezoidal wing model under consideration is assumed to behave as a thin plate of uniform mass and stiffness based on the von Kármán nonlinear plate theory. Rayliegh–Ritz method is used to transfer equations into modal domain to solve equations of motion. In accord with the Rayliegh–Ritz method (see Ref. 7) admissible functions must be selected so that geometric boundary conditions are satisfied. In the case of rectangular cantilever plates, the product of clamped–free and free–free beam functions are sufficient to satisfy geometric boundary conditions. Because of the nonregular boundary shape in a swept back trapezoidal plate and its associate difficulty to select admissible functions for vibration analysis, we mapped the trapezoidal domain into a unit square domain referred to the normalized beam coordinates. The following general formulation allows the treatment of a whole family of rectilinear wings of arbitrary constant taper and aspect ratios through the use of transformation to the normalized beam mode coordinates.

Wing taper ratio (TR), is defined as a ratio of the wing tip chord, c_t to the root chord c_r. The aspect ratio (AR), is defined in terms of c_r, TR, and semispan length L as

$$\mathrm{AR} = \frac{(\mathrm{span})^2}{\text{wing area}} = \frac{4}{1+\mathrm{TR}}\left(\frac{L}{c_r}\right) \tag{1}$$

To facilitate the use of clamped–free and free–free beam functions for approximating mode shapes of the plate and any wing fittings, transformations given as follows map any point from physical coordinates on the wing to the normalized beam coordinates:

$$\xi = \frac{x/c_r - (\mathrm{AR}/4)(1+\mathrm{TR})\tan\Lambda(y/L)}{1-(1-\mathrm{TR})y/L}, \qquad \eta = y/L \tag{2}$$

where Λ is sweep angle of the wing as shown in Fig. 1.

To approximate mode shapes of the plate to use the Rayliegh–Ritz method, products of clamped–free and free–free beam functions are selected as admissible functions given by Eq. (3). These equations give the transverse or out-of-plane displacement w and the in-plane displacements u and v at any point on the wing. They can be expressed as a time-dependent weighted sum of assumed spatial mode shape functions,

$$u(x,y,t) = \sum_i \sum_j u_i[\xi(x,y)] \times u_j[\eta(x,y)] a_{ij}(t)$$

$$v(x,y,t) = \sum_r \sum_s v_r[\xi(x,y)] \times v_s[\eta(x,y)] b_{rs}(t)$$

$$w(x,y,t) = \sum_m \sum_n \psi_m[\xi(x,y)] \times \phi_n[\eta(x,y)] q_{mn}(t) \tag{3}$$

Table 1 Approximate spatial wave numbers for free–free and clamped–free beam modes

i	α_i	j	β_j
3	4.7300407	1	1.8751041
4	7.8532046	2	4.6940911
5	10.995608	3	7.8532046
≥6	$(\pi/2)(2i+1)$	≥4	$(\pi/2)(2j-1)$

where $a_{ij}(t)$, $b_{rs}(t)$, and $q_{mn}(t)$ are generalized coordinates and the mode functions u_i, u_j, v_r, v_s, ϕ_m, and ψ_n can be obtained using exact solutions of beam as given by

$$u_i(\xi) = \cos(i\pi\xi), \qquad u_j(\eta) = \sin[(2j-1)/2]\pi\eta$$

$$v_r(\xi) = \cos(r\pi\xi), \qquad v_s(\eta) = \sin[(2s-1)/2]\pi\eta$$

$$\psi_1(\xi) = 1, \qquad \psi_2(\xi) = \sqrt{3}(1-2\xi)$$

$$\psi_m(\xi) = [\cos(\alpha_m x) + \cosh(\alpha_m x)] - \left[\frac{\cos(\alpha_m) - \cosh(\alpha_m)}{\sin(\alpha_m) - \sinh(\alpha_m)}\right] \times [\sin(\alpha_m x) + \sinh(\alpha_m x)] \qquad m \geq 3$$

$$\phi_n(\eta) = -[\cos(\beta_n\eta) - \cosh(\beta_n\eta)] - \left[\frac{\sin(\beta_n) - \sinh(\beta_n)}{\cos(\beta_n) + \cosh(\beta_n)}\right] \times [\sin(\beta_n\eta) - \sinh(\beta_n\eta)]$$

where ψ_n are the one-dimensional free–free beams modes in the chordwise direction of the plate and ϕ_m are the one-dimensional clamped–free beam modes in the spanwise direction. These functions are orthonormal over the range $0 \leq \xi, \eta \leq 1$ and have associated wave numbers computed as given in Table 1. Here, α_i and β_j are approximate special wave numbers for free–free and clamped–free beam modes, respectively.

In-Plane Equations

It is assumed that all of the nonconservative forces act only in the z direction and in-plane inertia may be neglected. Thus, the in-plane equations of motion are determined from the stretching strain energy and Lagrange's equation (see Ref. 8). The nondimensional in-plane u and v are given as:

$$\sum_k \sum_p C^{ij}_{kp} a_{kp} + \sum_g \sum_f C^{ij}_{gf} b_{gf} = C^{ij} \tag{4}$$

$$\sum_k \sum_p D^{rs}_{kp} a_{kp} + \sum_g \sum_f D^{rs}_{gf} b_{gf} = D^{rs} \tag{5}$$

where C^{ij}_{kp} and C^{ij}_{gf} is defined as given as follows and D^{rs}_{kp}, D^{rs}_{gf}, C^{ij}, and D^{rs} can be obtained in a similar way:

$$C^{ij}_{kp} = 2\left(\frac{h}{c_r}\right)^2 \int_0^1 u'_k u'_i \,\mathrm{d}\xi \int_0^1 E(\eta) v_p v_j \,\mathrm{d}\eta + (1-\nu)\left(\frac{h}{L}\right)^2 \left[\int_0^1 F(\xi)^2 u'_k u'_i \,\mathrm{d}\xi \int_0^1 E(\eta) v_p v_j \,\mathrm{d}\eta\right.$$

$$+\int_0^1 F(\xi)u_k'u_i\,\mathrm{d}\xi\int_0^1 v_p v_j'\,\mathrm{d}\eta+\int_0^1 F(\xi)u_k u_i'\,\mathrm{d}\xi\int_0^1 v_p' v_j\,\mathrm{d}\eta$$

$$+\int_0^1 u_k u_i\,\mathrm{d}\xi\int_0^1 v_p' v_j'\frac{\mathrm{d}\eta}{E(\eta)}\Bigg] \tag{6}$$

$$C_{gf}^{ij}=2\nu\left(\frac{h}{c_r}\right)\left(\frac{h}{L}\right)\int_0^1 F(\xi)u_g'u_i'\,\mathrm{d}\xi\int_0^1 v_f v_j\,\mathrm{d}\eta$$

$$+\int_0^1 u_g u_i'\,\mathrm{d}\xi\int_0^1 v_f' v_j\,\mathrm{d}\eta+(1-\nu)\left(\frac{h}{c_r}\right)\left(\frac{h}{L}\right)$$

$$\times\Bigg[\int_0^1 F(\xi)u_g'u_i'\,\mathrm{d}\xi\int_0^1 E(\eta)v_f v_j\,\mathrm{d}\eta$$

$$+\int_0^1 u_g'u_i\,\mathrm{d}\xi\int_0^1 v_f v_j'\,\mathrm{d}\eta\Bigg] \tag{7}$$

Here $F(\xi)$ and $E(\eta)$ are components of the Jacobian matrix and are defined by

$$F(\xi)=(1-\mathrm{TR})\xi-(\mathrm{AR}/4)(1+\mathrm{TR})\tan\Lambda$$

$$E(\eta)=1/[1-(1-\mathrm{TR})\eta] \tag{8}$$

Transverse Equations

The transverse equation is formed by substituting the kinetic and strain energy expressions into Lagrange's equation. The nondimensional equation is

$$\sum_m\sum_n\left\lfloor A_{mn}^{ij}\ddot{q}_{mn}(\tau)+B_{mn}^{ij}q_{mn}(\tau)\right\rfloor+Q^{ij}=-F_N \tag{9}$$

where A_{mn}^{ij} and B_{mn}^{ij} are coefficient terms defined as follows and in the Appendix, respectively, and Q^{ij} is the nondimensionalized generalized aerodynamic force that will be discussed in the next section:

$$A_{mn}^{ij}=\frac{1}{6}\int_0^1\phi_i\phi_m\,\mathrm{d}\xi\int\psi_j\psi_n\frac{\mathrm{d}\eta}{E(\eta)} \tag{10}$$

Aerodynamic Method: Vortex Lattice Model

The flow about the cantilever trapezoidal plate is assumed to be incompressible, inviscid, and irrotational. Here we use an unsteady vortex lattice method to model this flow. A typical planar vortex lattice mesh for the three-dimensional flow is shown in Fig. 1. The plate and wake are divided into a number of elements. Point vortices are placed on the plate and in the wake at the quarter chord of the elements. At the three-quarter chord of each plate element, a collocation point is placed for the downwash, that is, we require the velocity induced by the discrete vortices to equal the downwash arising from the unsteady motion of the plate. The aerodynamic matrix equation can be obtained as

$$A\boldsymbol{\Gamma}^{t+1}+B\boldsymbol{\Gamma}^{t}=w^{t+1} \tag{11}$$

where $\boldsymbol{\Gamma}^{t+1}$ is the strength vector of vortices and w^{t+1} is the downwash at the collocation points at step time of $t+1$. A and B are aerodynamic coefficient matrices given by Hopkins and Dowell.[1] From fundamental aerodynamic theory, we can obtain the pressure distribution on the trapezoidal plate at the jth point in terms of the vortex strength as:

$$\Delta\bar{p}_j=\frac{1}{\Delta\xi}\left[\frac{E(\eta)\left(\boldsymbol{\Gamma}_j^{t}+\boldsymbol{\Gamma}_j^{t+1}\right)}{2}+\sum_{i=1}^{j}\left(\boldsymbol{\Gamma}_i^{t+1}-\boldsymbol{\Gamma}_i^{t}\right)\right]$$

Aeroelastic State-Space Model

At this stage we can combine structural dynamics response with aerodynamic equations to obtain the aeroelastic model. Consider a discrete-time history of plate motion $q(t)$, with a constant sampling time step Δt. The sampled version of $q(t)$ and the velocity of this discrete-time series are defined by

$$q=(q^{t+1}+q^{t})/2,\qquad \dot{q}=(q^{t+1}-q^{t})/\Delta t \tag{12}$$

By the use of Eq. (12), the structural dynamic given by Eq. (9) can be reconstituted as a state-space equation in discrete-time form as

$$D_2\boldsymbol{\theta}^{t+1}+D_1\boldsymbol{\theta}^{t}+C_2\boldsymbol{\Gamma}^{t+1}+C_1\boldsymbol{\Gamma}^{t}=-F_N \tag{13}$$

where the vector $\{\boldsymbol{\theta}\}=\{\dot{q},q\}$ is the state of the plate and D_1 and D_2 are matrices describing the plate structural behavior. C_1 and C_2 are matrices describing the vortex element behavior on the plate itself and F_N is a nonlinear force due to large deflection of the plate.

There is a linear relationship between the downwash $\boldsymbol{w}$ at the collocation points and plate response $\boldsymbol{\theta}$ as $w=E\boldsymbol{\theta}$. Combining Eqs. (11) and (13), we obtain the aeroelastic state-space model in matrix form as

$$\begin{bmatrix}A & -E\\ C_2 & D_2\end{bmatrix}\begin{Bmatrix}\Gamma\\ \boldsymbol{\theta}\end{Bmatrix}^{t+1}+\begin{bmatrix}B & 0\\ C_1 & D_1\end{bmatrix}\begin{Bmatrix}\Gamma\\ \boldsymbol{\theta}\end{Bmatrix}^{t}=\begin{Bmatrix}0\\ -F_N\end{Bmatrix}^{t+\frac{1}{2}} \tag{14}$$

We refer to Eq. (14) as the complete discrete-time fluid/structure model. The eigenvalue solution of this discrete-time model determines the stability of the aeroelastic system in terms of eigenvalues z_i. If any of the eigenvalues have magnitude greater than unity, then the system is unstable. In principle, one could find the eigenvalues of Eq. (14) directly. However, for most aeroelastic calculations, one must compute the eigenvalues of the system as a function of some parameters, such as the variation of reduced velocity.

Numerical Results

Various types of swept back trapezoidal cantilever plate models of varying aspect ratios and TRs were considered. Each model is taken to be an aluminum alloy plate of constant thickness with different aspect ratios AR from 2 to 10. The wing root chord $c_r=0.365$ is fixed. The plate thickness h is 0.001 m, and Poisson's ratio ν is 0.3.

For the basic case, the plate was modeled using 50 vortex elements, that is, $km=10$ and $kn=5$. Here, kmm is selected to be 40, which gives 150 vortex elements for the wake model. The total number of vortex elements (or aerodynamic degrees of freedom) is 200. In the nonlinear limit-cycle analysis, where the time response of the system is investigated, there is a numerical instability (numerical divergence) at higher flow velocity for larger Δt or smaller km. In these cases, the plate was modeled using 100 vortex elements, that is, $km=20$ and $kn=5$, and the wake was modeled using 300 vortex elements, that is, $kmm=80$. The vortex relaxation factor was taken to be $\alpha=0.992$.

Stability of Aeroelastic Model

When the nonlinear force F_N in Eq. (14) is set to be zero, a linear aeroelastic model is obtained. The aeroelastic eigenvalue solutions of linear model determine the stability of the system. The discrete-time eigenvalues z_i are related to continuous-time eigenvalues λ_i by $z_i=\exp(\lambda_i\Delta t)$. When the real part of any eigenvalue λ_i becomes positive, the entire system becomes unstable. Figure 2 shows the eigenanalysis in the form of real eigenvalues, $\mathrm{Re}(\lambda)$ vs the flow velocity for sweep angles of leading edge of 0 and 30 deg. Figure 2b shows at 30 deg there is an intersection of $\mathrm{Re}(\lambda)$ with the velocity axis at $U_f=32$ m/s, which is the critical flutter velocity. In Fig. 2a, there are two intersections of $\mathrm{Re}(\lambda)$ with the velocity axis. One is $U_f=42$ m/s for the critical flutter velocity with the corresponding flutter oscillatory frequency 76.8 rad/s. The other is $U_d=54.3$ m/s for divergent velocity with zero oscillatory frequency. From Fig. 2b it is also found that in contrast to rectangular wings, for swept back wings, static instability (divergence) does not occur while the flutter

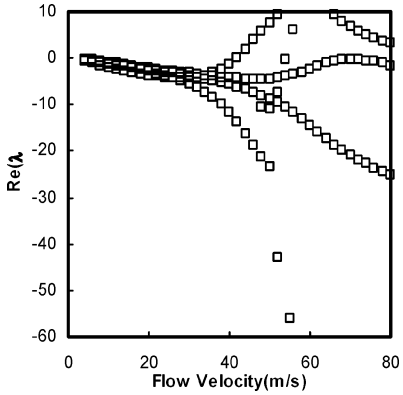

a)

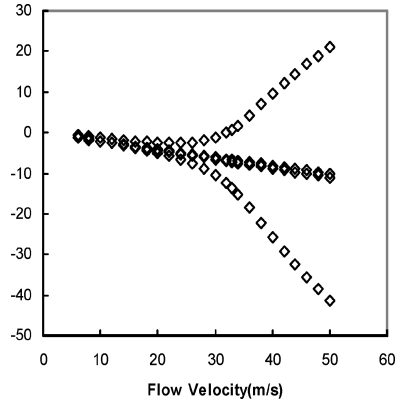

b)

Fig. 2 Eigenvalue solution for linear aeroelastic model for a) $\Lambda = 0$, rectangular and b) $\Lambda = 30$, trapezoidal.

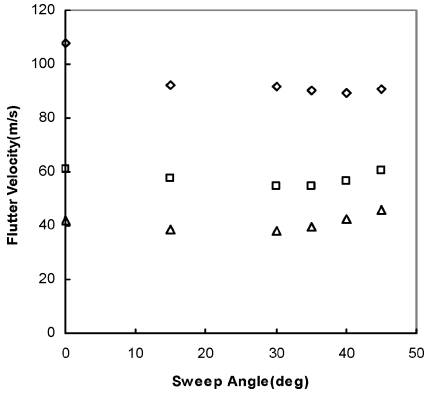

a)

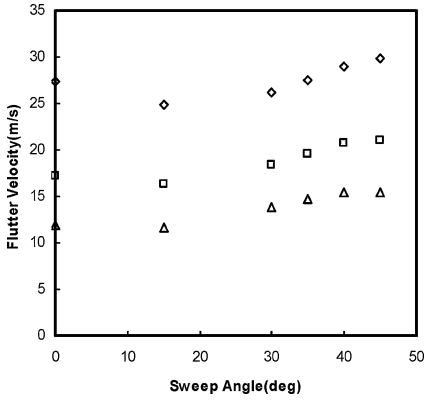

b)

Fig. 3 Flutter velocity vs sweep angle for a) AR = 4 and b) AR = 5: ◇, TR = 0.5; □, TR = 0.75; and △, TR = 1.0.

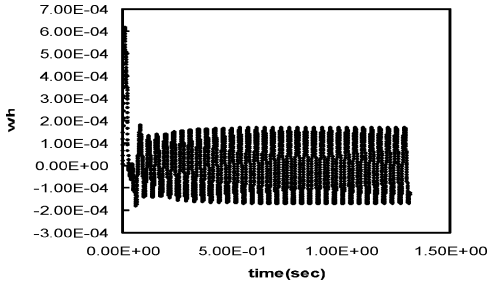

a) Nondimensional transverse deflection

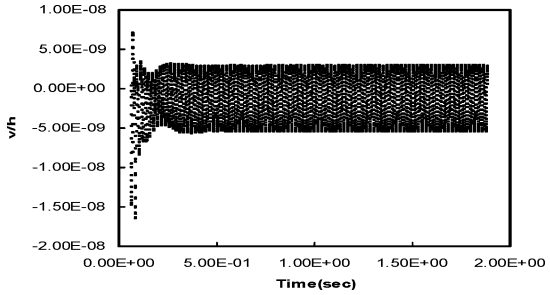

b) Nondimensional in-plane deflection

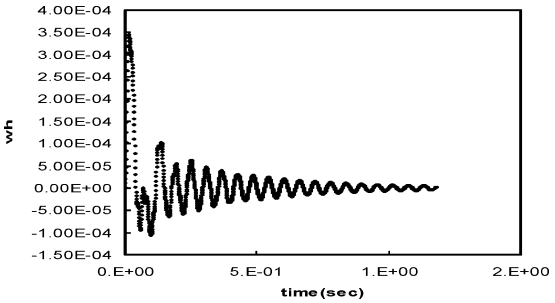

c) Decaying oscillation of the transverse deflection

Fig. 4 LCO for $U = 95$ m/s, $\Lambda = 30$, and TR = 0.5.

velocity decreases. The variation of flutter velocity vs sweep angle, for various TRs and aspect ratios is given in Figs. 3a and 3b. Figures 3a and 3b show that, in all cases, there is a minimum critical flutter velocity. For example, for AR = 4 and TR = 0.5, minimum flutter velocity is nearly 33.8 m/s. Figures 3a and 3b also show by increasing the TR from 0.5 to 1 for a given aspect ratio and sweep angle the flutter velocity decreases. For example, with AR = 4 and $\Lambda = 30$ deg, the flutter velocity decreases from 34 to 17.35 m/s.

Limit-Cycle Oscillation of Nonlinear Model

We have used a standard discrete-time algorithm to calculate the nonlinear response of this aeroelastic system. The full aeroelastic model [Eq. (14)] is used for a range of aspect ratio, sweep angle, and TR. The time step $\Delta t = c_r \times \Delta\xi / U$ is constant for a given flow velocity U. Typical nondimensional transverse and in-plane displacement time histories at location $\xi = 0.75$ and $\eta = 1$ for $U = 95$ m/s $> U_f$ (where $\Lambda = 30$ deg, TR = 0.5, and AR = 2) are shown in Figs. 4a and 4b. There are a steady-state limit-cycle oscillation (LCO) with frequency of 25.1 Hz. Note that the linear flutter velocities is $U_f = 91.75$ m/s. Figures 4 reveal that, because the plate deflects in both the positive and negative z directions, the in-plane displacement amplitudes u (and v) increase in the negative x (and y) directions. Thus, the maximum transverse displacements w, both positive and negative, correspond to the maximum negative in-plane displacements, and the in-plane displacements oscillate at twice the transverse oscillation frequency of 50.2 Hz. For a flow velocity lower than the linear flutter velocity, for example, at $U = 90$ m/s (where $\Lambda = 30$ deg, TR = 0.5, and AR = 2), the response decays to zero, as shown in Fig. 4c. Note that, if we were to change the sign of the initial conditions, then Fig. 4a would undergo a sign

reversal, but Fig. 4b would be unchanged because $u, v \sim w^2$. Figures 4a and 4b show that the limit-cycle response is on the order of the plate thickness well beyond the linear flutter velocity. When we calculated the LCO, we found that there is a numerical instability (numerical divergence) at higher flow velocity for larger Δx or (Δt) for smaller km, for example, when $km = 15$, the numerical divergence will occur when $U > 100$ m/s for $\Lambda = 30$ deg, TR $= 0.5$, and AR $= 2$, where $ny = 2$ and $nx = 4$. To obtain the LCO in the higher flow velocity range, we have to increase km and the corresponding kmm, for example, we used $km = 25$ and $kmm = 100$ for $ny = 2$ and $nx = 4$. We conclude this discussion by noting the correspondence of our theoretical results with the experimental results of Doggett and Soistmann.[9] These authors tested delta (triangular) wings with the lower sweep angles corresponding to higher aspect ratios and higher sweep angles corresponding to lower aspect ratios. For the last case they observed "limited amplitude oscillations."[9]

Conclusions

A trapezoidal cantilever plate and three-dimensional vortex lattice aerodynamic theory has been used to investigate the aeroelastic characteristics of a swept back trapezoidal wing in low subsonic flow. There are several parameters including sweep angle, TR, and aspect ratio that have considerable effect on aeroelastic behavior and characteristics of these wings. The results presented in this work are consistent with numerical results for low aspect ratio rectangular wings and experimental data for delta wings reported by other investigators (Refs. 3–9). This analysis can be used adequately for aircraft design procedures and estimation of the optimum aspect ratio, TR, and sweep angle of an aircraft wing especially at conceptual design stages.

Appendix: Expressions for C^{ij}, D^{rs}, D^{rs}_{kp}, D^{rs}_{gf} and B^{mn}_{ij}

For Eq. (4), the term C^{ij} is given as follows:

$$
\begin{aligned}
C^{ij} = -\sum_m\sum_n\sum_r\sum_s q_{mn}q_{rs}\Bigg\{&\left(\frac{h}{c_r}\right)^3\int_0^1 \phi'_m\phi'_r u'_t\,\mathrm{d}\xi \\
&\times\int_0^1 \psi_n\psi_x v_j\,\mathrm{d}\eta + \nu\left(\frac{h}{c_r}\right)\left(\frac{h}{L}\right)^2\Bigg[\int_0^1 F(\xi)^2\phi'_m\phi'_r u'_i\,\mathrm{d}\xi \\
&\times\int_0^1 E(\eta)^2\psi_n\psi_s v_f\,\mathrm{d}\eta + \int_0^1 \phi_m\phi_r u'_j\,\mathrm{d}\xi\int_0^1 \psi'_n\psi'_x v_j\,\mathrm{d}\eta \\
&+2\int_0^1 F(\xi)\phi'_m\phi_r u'_f\,\mathrm{d}\xi\int_0^1 E(\eta)\psi_n\psi'_s v_j\,\mathrm{d}\eta\Bigg] \\
&+(1-\nu)\left(\frac{h}{c_r}\right)\left(\frac{h}{L}\right)^2\Bigg[\int_0^1 F(\xi)^2\phi'_m\phi'_r u'_j\,\mathrm{d}\xi \\
&\times\int_0^1 E(\eta)^2\psi_n\psi_s v_j\,\mathrm{d}\eta + \int_0^1 F(\xi)\phi'_m\phi'_r u_j\,\mathrm{d}\xi \\
&\times\int_0^1 E(\eta)\psi_n\psi_s v'_j\,\mathrm{d}\eta + \int_0^1 F(\xi)\phi'_m\phi_r u'_j\,\mathrm{d}\xi \\
&\times\int_0^1 E(\eta)\psi_n\psi'_s v_f\,\mathrm{d}\eta + \int_0^1 \phi'_m\phi_r u_f\,\mathrm{d}\xi\int_0^1 \psi_n\psi'_s v'_j\,\mathrm{d}\eta\Bigg]\Bigg\}
\end{aligned}
$$

For Eq. (5), the terms D^{rs}, D^{rs}_{kp} and D^{rs}_{gf} are given as follows:

$$
\begin{aligned}
D^{rs} = -\sum_m\sum_n\sum_r\sum_s q_{mn}q_{rs}\Bigg\{&\left(\frac{h}{c_r}\right)^3\int_0^1 \phi'_m\phi'_r u'_i\,\mathrm{d}\xi \\
&\times\int_0^1 \psi_n\psi_s v_j\,\mathrm{d}\eta + \nu\left(\frac{h}{c_r}\right)\left(\frac{h}{L}\right)^2\Bigg[\int_0^1 F(\xi)^2\phi'_m\phi'_r u'_i\,\mathrm{d}\xi \\
&\times\int_0^1 E(\eta)^2\psi_n\psi_s v_j\,\mathrm{d}\eta + \int_0^1 \phi_m\phi_r u'_i\,\mathrm{d}\xi\int_0^1 \psi'_n\psi'_s v_j\,\mathrm{d}\eta \\
&+2\int_0^1 F(\xi)\phi'_m\phi_r u'_j\,\mathrm{d}\xi\int_0^1 E(\eta)\psi_n\psi'_s v_j\,\mathrm{d}\eta\Bigg] \\
&+(1-\nu)\left(\frac{h}{c_r}\right)\left(\frac{h}{L}\right)^2\Bigg[\int_0^1 F(\xi)^2\phi'_m\phi'_r u'_i\,\mathrm{d}\xi \\
&\times\int_0^1 E(\eta)^2\psi_n\psi_s v_j\,\mathrm{d}\eta + \int_0^1 F(\xi)\phi'_m\phi'_r u_i\,\mathrm{d}\xi \\
&\times\int_0^1 E(\eta)\psi_n\psi_s v'_j\,\mathrm{d}\eta + \int_0^1 F(\xi)\phi'_m\phi_r u'_j\,\mathrm{d}\xi \\
&\times\int_0^1 E(\eta)\psi_n\psi'_s v_f\,\mathrm{d}\eta + \int_0^1 \phi'_m\phi_r u_j\,\mathrm{d}\xi\int_0^1 \psi_n\psi'_s v'_j\,\mathrm{d}\eta\Bigg]\Bigg\}
\end{aligned}
$$

$$
\begin{aligned}
D^{rs}_{kp} = 2\nu\left(\frac{h}{c_r}\right)\left(\frac{h}{L}\right)\Bigg[&\int_0^1 F(\xi)u'_k u'_r\,\mathrm{d}\xi\int_0^1 E(\eta)v_f v_f\,\mathrm{d}\eta \\
&+\int_0^1 u'_k u_r\,\mathrm{d}\xi\int_0^1 v_p v'_j\,\mathrm{d}\eta\Bigg] + (1-\nu)\left(\frac{h}{c_r}\right)\left(\frac{h}{L}\right) \\
&\times\Bigg[\int_0^1 F(\xi)u'_k u'_r\,\mathrm{d}\xi\int_0^1 E(\eta)v_p v_s\,\mathrm{d}\eta \\
&+\int_0^1 u_k u'_r\,\mathrm{d}\xi\int_0^1 v'_p v_s\,\mathrm{d}\eta\Bigg]
\end{aligned}
$$

$$
\begin{aligned}
D^{rs}_{gf} = 2\left(\frac{h}{L}\right)^2\Bigg[&\int_0^1 F(\xi)^2 u'_g u'_r\,\mathrm{d}\xi\int_0^1 E(\eta)v_f v_s\,\mathrm{d}\eta \\
&+\int_0^1 F(\xi)u_g u'_r\,\mathrm{d}\xi\int_0^1 v_f v_s\,\mathrm{d}\eta + \int_0^1 F(\xi)u'_g u_r\,\mathrm{d}\xi \\
&\times\int_0^1 v_f v_s\,\mathrm{d}\eta + \int_0^1 u_g u_r\,\mathrm{d}\xi\int_0^1 v'_f v'_s\frac{\mathrm{d}\eta}{E(\eta)} \\
&+(1-\nu)\left(\frac{h}{c_r}\right)^2\int_0^1 u'_g u'_r\,\mathrm{d}\xi\int_0^1 E(\eta)v_f v_s\,\mathrm{d}\eta\Bigg]
\end{aligned}
$$

For Eq. (9), the term B^{ij}_{mn} is given as follows:

$$
\begin{aligned}
B^{ij}_{mn} = \frac{1}{6}\Bigg\{&\int_0^1 \phi^m_i\phi^n_m\,\mathrm{d}\xi\int_0^1 E(\eta)^2\psi_j\psi_n\,\mathrm{d}\eta \\
&+\left(\frac{c_r}{L}\right)^4\Bigg[\int_0^1 F(\xi)^2\phi^m_i\phi^n_m\,\mathrm{d}\xi\int_0^1 E(\eta)^3\psi_j\psi_n\,\mathrm{d}\eta \\
&+4\int_0^1 F(\xi)^2\phi'_i\phi'_m\,\mathrm{d}\xi\int_0^1 E(\eta)\psi'_j\psi'_n\,\mathrm{d}\eta + \int_0^1 \phi_i\phi_m\,\mathrm{d}\xi \\
&\times\int_0^1 E(\eta)\psi^n_j\psi^m_n\,\mathrm{d}\eta + 2\int_0^1 F(\xi)^3\phi^n_i\phi'_m\,\mathrm{d}\xi \\
&\times\int_0^1 E(\eta)^2\psi_j\psi'_n\,\mathrm{d}\eta + 2\int_0^1 F(\xi)^2\phi'_i\phi^n_m\,\mathrm{d}\xi
\end{aligned}
$$

$$\times \int_0^1 E(\eta)^2 \psi_f' \psi_n \,\mathrm{d}\eta + \int_0^1 F(\xi)^2 \phi_i^n \phi_m \,\mathrm{d}\xi \int_0^1 E(\eta) \psi_j \psi_n^m \,\mathrm{d}\eta$$

$$+ \int_0^1 F(\xi)^2 \phi_i \phi_m^n \,\mathrm{d}\xi \int_0^1 E(\eta) \psi_j^n \psi_n \,\mathrm{d}\eta + 2 \int_0^1 F(\xi) \phi_i' \phi_m \,\mathrm{d}\xi$$

$$\times \int_0^1 E(\eta) \psi_j' \psi_n^m \,\mathrm{d}\eta + 2 \int_0^1 F(\xi) \phi_j \phi_m' \,\mathrm{d}\xi \int_0^1 \psi_j^n \psi_n' \,\mathrm{d}\eta \Bigg]$$

$$+ \nu \left(\frac{c_r}{L}\right)^2 \Bigg[\int_0^1 F(\xi)^2 \phi_j^m \phi_m^n \,\mathrm{d}\xi \int_0^1 E(\eta)^3 \psi_j \psi_n \,\mathrm{d}\eta$$

$$+ 2 \int_0^1 F(\xi) \phi_i' \phi_m^n \,\mathrm{d}\xi \int_0^1 E(\eta)^2 \psi_j' \psi_n \,\mathrm{d}\eta + \int_0^1 \phi_j^n \phi_m \,\mathrm{d}\xi$$

$$\times \int_0^1 E(\eta) \psi_j \psi_n^m \,\mathrm{d}\eta + \int_0^1 F(\xi)^2 \phi_i^m \phi_m^n \,\mathrm{d}\xi \int_0^1 E(\eta)^3 \psi_j \psi_n \,\mathrm{d}\eta$$

$$+ 2 \int_0^1 F(\xi) \phi_i' \phi_m^n \,\mathrm{d}\xi \int_0^1 E(\eta)^2 \psi_j' \psi_n \,\mathrm{d}\eta + \int_0^1 \phi_i \phi_m^n \,\mathrm{d}\xi$$

$$\times \int_0^1 E(\eta) \psi_j^n \psi_n \,\mathrm{d}\eta \Bigg] + 2(1-\nu) \left(\frac{c_r}{L}\right)^2 \Bigg[\int_0^1 F(\xi)^2 \phi_i^n \phi_m^n \,\mathrm{d}\xi$$

$$\times \int_0^1 E(\eta) \psi_j \psi_n \,\mathrm{d}\eta + \int_0^1 \phi_i' \phi_m' \,\mathrm{d}\xi \int_0^1 E(\eta) \psi_j' \psi_n' \,\mathrm{d}\eta$$

$$+ \int_0^1 F(\xi) \phi_i^n \phi_m' \,\mathrm{d}\xi \int_0^1 E(\eta) \psi_j \psi_n' \,\mathrm{d}\eta$$

$$+ \int_0^1 F(\xi) \phi_j' \phi_m^n \,\mathrm{d}\xi \int_0^1 E(\xi)^2 \psi_j' \psi_n \,\mathrm{d}\eta \Bigg] \Bigg\}$$

References

[1]Hopkins, M. A., and Dowell, E. H., "Limited Amplitude Panel Flutter with a Temperature Differential," *Proceeding of the AIAA/ASME/ASCE/AHS/ASC 35th Structures, Structural Dynamics, and Materials Conference*, AIAA, Washington, DC, 1994, pp. 1343–1355.

[2]Weiliang, Y., and Dowell, E. H., "Limit-Cycle Oscillation of a Fluttering Cantilever Plate," *AIAA Journal*, Vol. 32, No. 12, 1994, pp. 2426–2432.

[3]Tang, D. M., Dowell, E. H., and Hall, K. C., "Limit-Cycle Oscillations of a Cantilevered Wing in Low Subsonic Flow," *AIAA Journal*, Vol. 37, No. 3, 1999, pp. 364–371.

[4]Tang, D. M., Henry, J. K., and Dowell, E. H., "Limit-Cycle Oscillations of a Delta Wing Model in Low Subsonic Flow," *AIAA Journal*, Vol. 37, No. 11, 1999, pp. 1355–1362.

[5]Bakhtiari-Nejad, F., and Shokrollahi, S., "Aeroelastic Eigenanalysis of a Cantilever Plate in Low Subsonic Flow to Predict Flutter Onset," *Proceedings of the 10th International Mechanical Engineering Conference*, Iranian Society of Mechanical Engineering (ISME), Tehran, May 2002.

[6]Bakhtiari-Nejad, F., Shokrollahi, S., and Dardel, M., "Effect of Local Forcing Functions on Flutter Suppression of a Low Aspect Ratio Rectangular Cantilever Plate," *Proceedings of the Ninth International Congress on Sound and Vibration*, Orlando, FL, July 2002.

[7]Meirovitch, L., *Principles and Techniques of Vibrations*, Prentice–Hall International Inc., 1997, pp. 522–531.

[8]Dowell, E. H., *Aeroelasticity of Plates and Shells*, Noordhoff International Publ., Leyden, The Netherlands, 1975, pp. 35–49.

[9]Doggett, R. V., and Soistman, D. L., "Some Low-Speed Flutter Characteristics of Simple Low-Aspect-Ratio Delta Wing Models," NASA TM-101547, Jan. 1989.

High-Order Compact Difference Scheme Applied to Double-Delta Wing Vortical Flows

Tomoyuki Arasawa*
Yokohama National University, Kanagawa 240-8501, Japan
Kozo Fujii†
Japan Aerospace Exploration Agency, Kanagawa 229-8510, Japan
and
Koji Miyaji‡
Yokohama National University, Kanagawa 240-8501, Japan

I. Introduction

DELTA wings are suitable for modern high-speed aircrafts due to the low drag at transonic and supersonic regimes. Indeed, a double-delta wing is especially favored because it has mixed characteristics of simple delta wings with small to large leading-edge swept-back angles. The performances of delta wings at landing or takeoff conditions are unfavorable because they require high angles of attack to attain necessary lifts at low speeds. The characteristics of delta wings for such flow conditions are governed by the leading-edge separation vortices over the wing. A number of investigations have been carried out for simple delta wings. From the viewpoint of numerical simulations, fairly accurate predictions are possible by today's computational fluid dynamics technique for low to moderately high angles of attack, that is, before vortex breakdown or lift stall occurs. On the other hand, there have not been sufficient studies on the flow over a double-delta wing despite their practical importance. Numerical accuracy for the problem has not been validated. Two vortices exist for each side of a double-delta wing; one is originating from the leading edge of the strake and the other from the main wing. These vortices interact with each other and eventually merge downstream. Thus, the flows over a double-delta wing are more complex than over a simple delta wing. In our previous effort,[1] the effects of grid resolution were examined by using fairly fine grids, but the results were not satisfactory when compared with the experiment,[2] even with the finest grid using 8 million points.

The purpose of this study is to improve the reliability of the numerical simulations of a double-delta wing using a high-order compact difference scheme.[3] It is a family of spatially implicit schemes, a subset of which are the well-known Padé approximations. The scheme is easily extended to higher-order accuracy with a small number of stencils and it has spectrallike resolutions. Its effectiveness have been reported in recent years for computational aeroacoustics, for example, where sound waves with small pressure fluctuations need to be captured accurately. In this paper, as the most standard scheme today, Roe's upwind scheme[4] is also used. The

Presented as Paper 2003-3537 at the AIAA 16th Computatinal Fluid Dynamics Conference, Orlando, FL, 23 June 2003; received 13 July 2003; revision received 4 January 2004; accepted for publication 12 January 2004.

*Graduate Student, Department of Environment and System Sciences, 79-5 Tokiwadai, Hodogaya, Yokohama.

†Professor, Institute of Space and Astronautical Sciences, 3-1-1 Yoshinodai, Sagamihara. Associate Fellow AIAA.

‡Lecturer, Department of Ocean and Space System Engineering, 79-5 Tokiwadai, Hodogaya, Yokohama. Member AIAA.